DIGITAL FILTERS FOR INTERFEROMETRIC INERTIAL SENSORS THAT USE OPTICAL PHASE MODULATION

Lidia Hissae Shibuya, lishibuya@uol.com.br
ITA – Instituto Tecnológico de Aeronáutica – Praça Marechal Eduardo Gomes, 50 – Vila das Acácias; CEP 12.228-900 – São José dos Campos – SP – Brasil

Ricardo Teixeira de Carvalho, ricardo@ieav.br
IEAv – Instituto de Estudos Avançados – Rodovia dos Tamoios, km 5.5 – Putim; Cep 12.228-001 – São Jose dos Campos – SP – Brasil

Osamu Saotome, osaotome@ita.br
ITA – Instituto Tecnológico de Aeronáutica – Praça Marechal Eduardo Gomes, 50 – Vila das Acácias; CEP 12.228-900 – São José dos Campos – SP – Brasil

Abstract. *Interferometric sensors, such as the fiber optic gyroscope, are made of a optical circuit where optical phase modulation is used to encode the phase measurement being made. The spectrum of the resulting photodetector signal contains harmonics from which rotation rates are measured. However, very precise sensors should be able to measure very small rotaion rates accurately, so that very small harmonic amplitudes are to be extracted from noise and in the presence of other much larger harmonic contents. We discuss and present the results related to the application of digital filtering technique based on a Morlet wavefunction, used in wavelet signal processing, in accomplishing such task, pointing out its advantadges and limitations with respect to traditional demodulation schemes.*

Keywords*: digital filters, fiber optic gyroscopes, Morlet wavelets*

1. INTRODUCTION

The ability of finding the exact position of a vehicle in space with respect to a reference frame is a key element which has allowed all the known feats in space and defense areas. In space, star position based sensors are important for satellite control. For vehicle navigation purposes, in particular, strap-down inertial sensors have been intensively researched to obtain very precise inertial navigation systems (INS) assembled in the vehicle. Those sensors are sets of accelerometers and gyrometers, and sometimes include other forms of navigation aid, such as the use of GPS data, satellite images, or other velocity or position sensors, to obtain, in combination with the original INS readings, better position estimates by using stochastic estimators such Kalman Filters (Farrel, 1998). A key element in INS systems is the gyrometer, which measures vehicle angular rotation rates along pre-defined mutually orthogonal axes. Gyrometers can be made on completely different technologies nowadays. A more compact hardware is obtained using commercial MEMS devices, which so far offers poorer performance compared to other well-established technologies. Mechanical gyros are precise mainstream devices, challenged by laser gyros and fiber-optic gyros (FOG). The rotation rate information allows, through integration, the estimation of angles between the coordinate frame in the vehicle, where the gyros and accelerometers are assembled, with respect to the Lab reference frame. These angles, which comprises the so called vehicle attitude data, are used so that vehicle acceleration components, measured at the vehicle frame, can also be computed in the Lab frame, and, through double integration, the position respect to this frame of reference is found. Since the gyro data is employed in three successive integrations, the impact on the INS performance of gyro errors is of greater concern than those derived from acceleration data errors, which pass through double integration. If t is the time of flight, one can say roughly that the position error variance derived only from integration of gyro inaccuracies grows much faster (proportional to t^3) than the variance derived from accelerometer errors only (proportional to t^2). So it has always been important to improve the measurement of vehicle rotation rates by reducing gyro output noise and drift. In this work, we are interested in the FOG device, in particular on enhancing its demodulation electronics performance as well as integrating its entire signal processing functions. The target is space applications, where tiny cargo space, low power consumption and robustness are of key concern. For that we propose and analyze a different approach to synthesize digital filters based on Morlet wavelet functions to be employed in the FOG electronics. Wavelets have been used for noise reduction in inertial sensors (Sheimy et al., 2004). Here we use it to extract very low amplitude harmonics in the presence of others which could even be 100 dB larger. The careful analysis of the proposed scheme is therefore of essence to determine the best signal-to-noise (SNR) achievable. The implementation, limitations and the optimization of filter parameters are also discussed.

2. THEORETICAL BACKGROUND

FOG´s are basically fiber-optic interferometric sensors (see Fig. 1): a lightwave coming from a light source feeds a bidirectional fiber coupler connected to a loop made of many turns of monomode optical fiber. The coupler splits

equally the incoming light into two counter-propagating light beams, making them travel in the loop. They are recombined at the same coupler, which is also the loop exit, and the resulting beam is shone upon a photodetector, where in general the effect of an eventual net phase difference ϕ_S experienced by the beams in the loop can be detected.

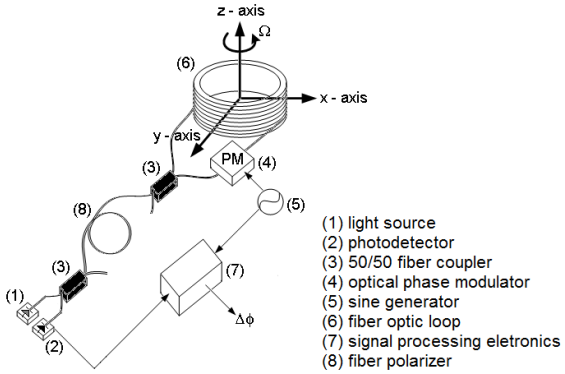

Figure 1. A basic FOG device: a Sagnac interferometer, made of fiber-optic loop, light source and directional couplers

In such configuration, a rotation rate Ω on the loop plane induces such optical phase difference ϕ_S, due to the Sagnac effect (Sagnac, 1913), (Post, 1967) and (Ezekiel and Arditty, 1982):

$$\phi_S = \left(\frac{2\pi LD}{\lambda c_0}\right) \times \Omega = k \times \Omega \tag{1}$$

here D is the loop diameter, L is the loop length, λ is the light wavelength, and c_0 is the vacuum light speed. The term in the brackets is known as the optical scale factor k. The interferometer is sensitive only to rotation rates in the direction perpendicular to the loop plane, which then defines the axis of rotation being sensed. A set of three mutually orthogonal fiber loops is a 3-D gyro set, usually with their axes aligned to the accelerometer set axes in the vehicle. The signal on the photodetector will be, as for interferometers, proportional to $cos^2(\phi_S/2)$, where $\phi_S = k\Omega$ and the interfering light beams are supposed here to be monochromatic beams. At very low rotation rates, though, operation of key interest here, the sensitivity is zero, since that function has derivative equal to zero at $\Omega \approx 0$. Besides, cos^2 function is an even function, and such system as described would not be able to discern a CW (clockwise) rotation rate from the same amplitude CCW (counter-clockwise) one, unless an optical phase modulation scheme be applied and (Ezekiel and Arditty, 1982) and (Vali and Shorthill, 1976). This would in turn solve another issue: the photodetector signal is a slow varying signal, almost "DC-like", for low angular acceleration rates, and it can be degraded by electronic *1/f noise*.

In order to overcome these problems above, an optical phase modulator (PM) must be inserted as part of the loop circuit, at one of the loop exits. PM´s could be a piezoelectric cylinder, so that the fiber can be wound around it. An external electrical modulation signal causes its mechanical expansion and contraction, and this in turn changes the wound fiber path length and/or its refractive index *n*. A PM may also be an integrated optics (OI) waveguide, made of an electro-optic material, spliced into the fiber loop, so that the waveguide refractive index changes following an external electrical signal. Piezoelectric PM´s are narrowband mechanical devices as opposed to OI ones, so they are often employed in open-loop configurations (Carvalho, 1991), where optical phases are directly read by the demodulation electronics. OI PM´s find good use in closed-loop systems (Lefèvre, 1993). There the system operates in zero total optical phase unbalance, since the PM is driven by an electrical signal as to generate an optical phase difference (between the counter-propagating beams) to oppose that induced by rotation via Sagnac effect. Thus that signal is an indirect measurement of how much the rotation rate is. Considering the phase modulation scheme using narrowband piezoelectric PM´s, the proper modulation signal in this case is a sinewave, with amplitude A_m, in Volts, and frequency ω_m. Now the total optical phase difference between the interfering light beams is the sum of the rotation-induced phase ϕ_S plus the time-varying phase difference introduced by the PM. This latter is due to the fact that the PM optical length is time-varying, and the CW and CCW beams arrive at the PM site at different instants separated by the loop travel time $\tau = nL/c_0$. The AC-coupled signal $V(t)$ seen on the photodetector is

$$V(t) = K\cos^2\left(\frac{\phi_S}{2} + \frac{\theta_m}{2} sin(\omega_m t)\right), \tag{2}$$

Here K is the general gyro scale factor, which is a product of the optical scale factor k defined before, the electronic gain of the photodetector/demodulation circuit, and the light source power. The amplitude

$$\theta_m = 2.H(\omega_m).A_m.sin\left(\frac{\omega_m \tau}{2}\right) \tag{3}$$

is the modulation index, and $H(\omega_m)$ is the transfer function of the piezoelectric PM at ω_m. We note that θ_m can be maximized by the proper choice of ω_m with respect to the loop transit time τ. The signal $V(t)$ has many harmonics multiples of ω_m. Taking into account only the most significant harmonics amplitudes, we may say that

$$V(t) \approx V_{1H}\, sin(\omega_m t) + V_{2H}\, cos(2\omega_m t) + V_{4H}\, cos(4\omega_m t) \tag{4}$$

The amplitudes V_{1H}, V_{2H} and V_{4H}, for small values of Ω, are proportional to Bessel functions of the index θ_m :

$$\begin{aligned} V_{1H} &= KJ_1(\theta_m) * sin(k\Omega) \approx KJ_1(\theta_m) * k\Omega \\ V_{2H} &= KJ_2(\theta_m) * cos(k\Omega) \approx KJ_2(\theta_m) \\ V_{4H} &= KJ_4(\theta_m) * cos(k\Omega) \approx KJ_4(\theta_m) \end{aligned} \tag{5}$$

A plot of typical FOG signals to be demodulated are shown in Figure 2. For $\Omega \approx 0$ the very small amplitude of the first harmonics, V_{1H}, is the measurement to be made, since it is proportional to Ω. However, this has to be accomplished in the presence of much larger harmonics V_{2H} and V_{4H}, so a band-pass filter approach should use very high Q filtering.

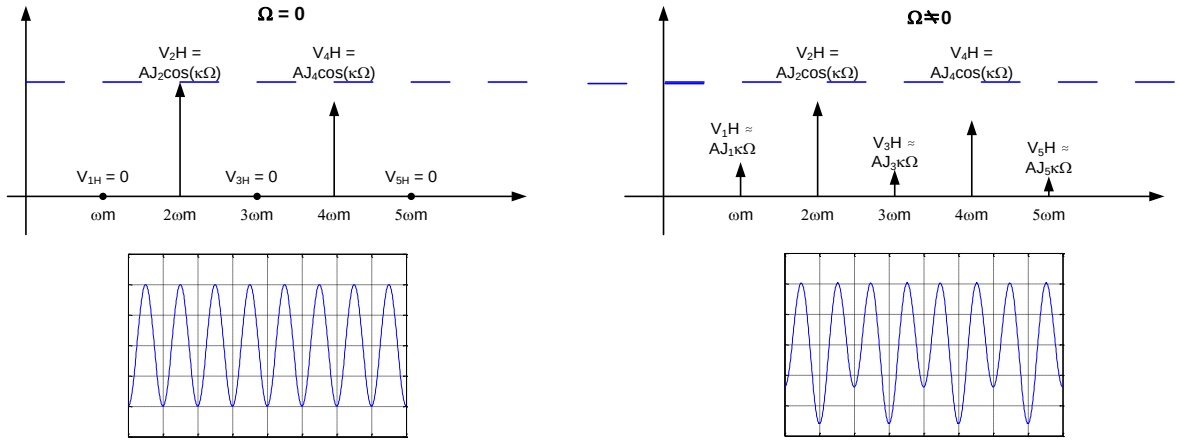

Figure 2. Typical FOG signals when optical phase modulation is used. Left: AC-coupled photodetector signal (lower) and its corresponding spectrum (up), for $\Omega = 0$. Right: the signal and its spectrum for $\Omega \neq 0$.

A traditional way of measuring V_{1H} is using a lock-in amplifier for synchronous detection, Fig. 3. There a sample of the modulation signal $A_m \sin(\omega_m t + \varphi)$ is made to mix to $V(t)$, and the result is low-pass filtered. After adjustment on the relative phase between those electrical signals we end up with a signal which is proportional to V_{1H}. For the custom electronics needed by a very precise gyro set, such analog lock-in circuit would suffer from sensitivity to environmental perturbations. Besides it demands that the sinusoidal signal applied to the PM must have very low distortion levels, since a spurious however small second harmonics content in this modulation signal may beat with the relatively much larger second harmonics of $V(t)$, introducing unacceptable levels of drift in the demodulation scheme. Such problem is illustrated in Fig. 3, where a simulated small random second harmonics distortion on the modulation signal shows the resulting drift in the demodulated output in a lock-in amplifier for $\Omega \approx 0$.

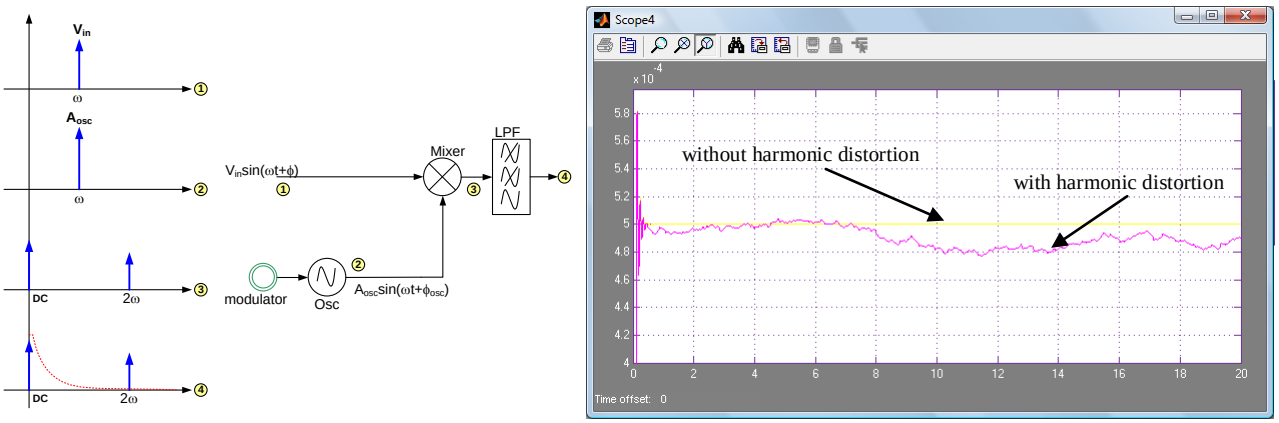

Figure 3. Left we see the lock-in demodulation scheme, and to the right drift caused by harmonics distortion.

A further concern to an analog lock-in approach is that one needs a circuit for each gyro, which makes more difficult FOG designs for miniaturized applications.

3. DIGITAL FILTERS BASED ON MORLET WAVELET FUNCTIONS

Figure 4 shows the Morlet wavelet functions, cosine (ψ_c) and sine (ψ_s) types. Their appearance is of oscillations encased into a gaussian envelope. They are one of many functions which can perform digital data analysis due to their intrinsic properties. Their mathematical description in a digitalized form is

$$\psi_c(f,n) = G_c \times e^{-\frac{(n-n_0)^2}{a}} \times cos(2.\pi.f.n.\delta t) \tag{6}$$

$$\psi_s(f,n) = G_s \times e^{-\frac{(n-n_0)^2}{a}} \times sin(2.\pi.f.n.\delta t) \tag{7}$$

so they are functions of the frequency f and time $t = n.\delta t$, where n marks the nth sample taken each small time interval δt, which is the inverse of the sample frequency. Number n_0 is the center sample, G_c and G_s are normalizing gains such that their dot product integrals over $(-\infty, +\infty)$ are 1.

$$\langle \psi_{sc}, \psi_c^* \rangle = \int_{-\infty}^{+\infty} \psi_c(t).\psi_c^*(t)dt = 1 \quad and \quad \langle \psi_s, \psi_s^* \rangle = \int_{-\infty}^{+\infty} \psi_s(t).\psi_s^*(t)dt = 1 \tag{8}$$

The parameter a determines how fast the Gaussian envelope dies out. One may extract amplitude and phase information of a particular spectral component of a digitalized signal $V(t)$ by taking the digitalized form of its dot product integral with the wavelet functions:

$$A_c(f) = \sum_{n=-\frac{n_{max}}{2}}^{\frac{n_{max}}{2}} \psi_c(f,n) \times V(n.\delta t) \tag{9}$$

$$A_s(f) = \sum_{n=-\frac{n_{max}}{2}}^{\frac{n_{max}}{2}} \psi_s(f,n) \times V(n.\delta t) \tag{10}$$

Here n_{max} is the number of points in the window been calculated, since we do it preferably in the points that lie inside the wavelet, before its gaussian envelope dies out. The desired amplitude is $\sqrt{A_c^2 + A_s^2}$.

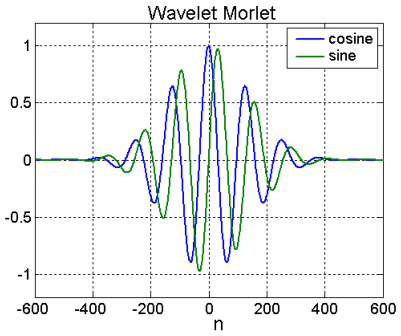

Figure 4. Morlet wavelet functions

While performing these sums, when $V(t)$ has many spectral components, signal components which are way off the chosen value f for the wavelet functions, either much larger or much smaller than f, do not add up cumulatively, whereas the integral on the signal component exactly at the wavelet frequency f may grow if in phase with either ψ_c or ψ_s oscillations. In this sense is that such operation can be seen as a band-pass filtering, applied to the signal been analyzed. However, in order to have that calculation produce a precise amplitude result, it is necessary that

$$\int_{-\infty}^{+\infty} \psi_s(t)dt = 0 \quad and \quad \int_{-\infty}^{+\infty} \psi_c(t)dt = 0 \tag{11}$$

which can be put in these terms: the DC component in the signal should not produce a net result in the calculation, whatever value it has. The first integral is always zero, since ψ_s is an odd function. For the function ψ_c, the above integral may approach zero, depending on the choice of a as related to the wavelet oscillation frequency f, but is not exactly zero:

$$\int_{-\infty}^{+\infty} \psi_c(t)dt = \sqrt{\pi a}.e^{-a\pi^2 f^2} = \sqrt{\pi a}.\beta(f) \tag{12}$$

This can lead to some small errors on the amplitude estimation, depending on how small the parameter $\beta(f) = e^{-a\pi^2 f^2}$ defined above is. We note that the normalization constants for the Morlet functions become

$$G_c = \frac{G}{\sqrt{1+\beta^2(f)}} \quad and \quad G_s = \frac{G}{\sqrt{1-\beta^2(f)}} \; with \; G = 1{,}128379 * a^{-\frac{1}{4}} \tag{13}$$

With the proper choice of a, we have $\beta^2(f) \approx 0$ and $G_c \approx G_s \approx G$. In order to evaluate the effect of $\beta(f)$, assume that we want by this filter approach to obtain the amplitude of a sinusoidal signal $v(t) = A.\sin(2\pi.f'.t + \phi)$. If we choose the wavelet parameter f as not necessarily equal to f', the integral dot product integrals as proposed above lead to

$$\langle \psi_s, v \rangle = \frac{A.G_s}{2}.\sqrt{\pi a}.\left(\beta(f' - f) - \beta(f' + f)\right).cos(\phi) \tag{14}$$

$$\langle \psi_c, v \rangle = \frac{A.G_c}{2}.\sqrt{\pi a}.\left(\beta(f' - f) + \beta(f' + f)\right).sen(\phi) \tag{15}$$

If we call $\hat{A}$ the calculated amplitude by the filter procedure, we end up with

$$\hat{A} = A.\sqrt{\frac{\beta^2(f'-f)+\beta^2(f'+f)-\left(2cos\,(2\phi).\beta(f'-f).\beta(f'+f)\right)}{1+\beta^4(f)}} \tag{16}$$

so that the calculation will not give the desired value A, since the signal and wavelet oscillation are not at same frequency. We point out that $\hat{A} \ll A$, since all β terms above are usually $\ll 1$, except at zero. However, if we make $f' = f$, $\beta(0) = 1$. If we chose the parameter a to be such that $\beta(mf) \approx 0$, being m any integer =1,2,3…, or else, $\beta^2(mf) < \varsigma$, where ς is a very small number as to ascertain the desired precision on the amplitude A, we get that

$$\hat{A} \cong A \tag{17}$$

so we may say that the wavelet oscillation frequency f defines the center of the filter bandwidth. The criteria to choose a as to have a very good estimation is

$$af^2 > \frac{ln\left(\frac{1}{\varsigma}\right)}{2\pi^2} \tag{18}$$

for example, if $\varsigma = 10^{-16}$, we may satisfy that condition for $af^2 > 1.86$. The expression for $\hat{A}$ can also lead us to the expression for the filter bandwidth. By replacing f' by $(f + \delta f)$, and since the center of the filter bandwidth is given by the chosen value of f, one may obtain the plot bellow as a function of δf, having $f = 1$ and a as a parameter:

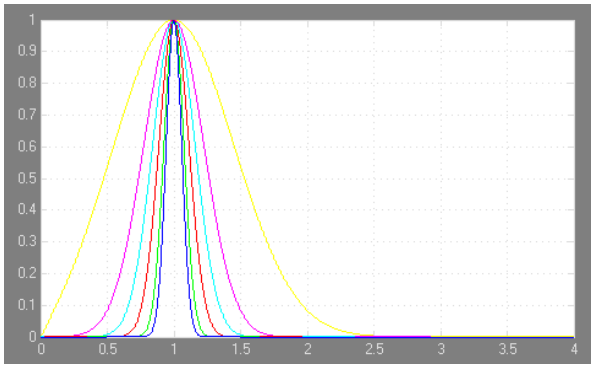

Legend

a	$2\Delta f$	color
0,25	0,78Hz	Yellow
1	0,38Hz	Pink
2	0,27Hz	Ciano
4	0,19Hz	Red
9	0,12Hz	Green
15	0,10Hz	Blue

Figure 5. Digital band pass filter gain curves for the Morlet function processing, having a as the parameter. Larger value of a implies in smaller bandwidth, or higher selectivity parameter $Q = f/\Delta f$ values.

For that, we can easily show that the equivalent filter bandwidth ($(f \pm \Delta f)$ at $1/\sqrt{2}$ of its maximum gain) is given by

$$2\Delta f = 2\sqrt{\frac{ln\sqrt{2}}{a\pi^2}} \tag{19}$$

We observe that the Morlet filter is in fact a true band pass filter, as opposed to digital filters which presents periodic bands in a comb like structure. Such digital filters are not good to be used in the FOG signal processing due to the presence of much larger harmonics contents with respect to the desired first harmonics.

4. FILTER APPLICATION TO THE FOG´s

If for the FOG signal $V(t)$ we take only the first and the second harmonics, with nominal amplitudes V_{1H} and V_{2H}, respectively, the gyro signal is

$$V(t) \cong V_{1H}\, sen(2\pi.f.t+\theta) + V_{2H}\, cos(4\pi.f.t+2\theta) \tag{20}$$

the calculated amplitude $\hat{V}_{1H}$ using the Morlet filter is:

$$\hat{V}_{1H} \;= V_{1H.}\sqrt{1+\left(\frac{V_{2H}}{V_{1H}}\right)^2\beta^2(f) - 2\beta(f)\left(\frac{V_{2H}}{V_{1H}}\right)sin\theta} \tag{21}$$

One may note that $\hat{V}_{1H} \cong V_{1H.}$ if V_{2H} is not as large respect to V_{1H} as to offset in the product the small values of $\beta(f)$ and $\beta^2(f)$. Therefore, for FOG applications, care has to be taken as to ascertain that this is so, in particular because at very low rotation rates usually $V_{2H} \gg V_{1H}$.

Our approach to FOG demodulation is to digitalize the gyro output $V(t)$ and then perform such calculation on a DSP processor. We do that at intervals Δt, obtaining successive gyro rotation rate samples, so that Δt defines the sensor bandwidth $B < 1/(2\Delta t)$. Also we note that $\Delta t = n_{max}\,.\,\delta t$, with the function centered on the interval Δt. Here we note that the choice of the parameter a with respect to the calculation window size Δt will be related to how precise the amplitude measurement is made. The theory predicts that we should perform an integral over all times, but in practical terms we do so within the window boundaries, which may cause a windowing effect. On the other hand, for larger values of *a*, our wavelet function is not totally inside the calculation window, so that we may miss significant parts of the integral. A study of those issues take us, quantitatively to evaluate how bad it is if we do not perform the dot product integrals over $(-\infty,+\infty)$. If we call $x = \frac{n_{max}}{2} * \delta t$ and $-x = -\frac{n_{max}}{2} * \delta t$ as the window time edges, so that the window size is *2.x*, we should evaluate the value of

$$\frac{\langle \psi_c, v\rangle_x}{\langle \psi_c, v\rangle} \tag{22}$$

where $\langle \psi_c, v\rangle_x$ is the dot product integral truncated at $(-x,+x)$. The signal v(t) to be analyzed can be any signal, but any desired spectral component to be measured is sinusoidal and its product with the term $cos(2\pi ft)$of the wavelet turns out to be also a sinewave. So a useful thing to do in order to compute the dot product ratio above is to create the function $\gamma(x,f)$, which evaluates the ratio of integrals only on the wavelet itself:

$$\frac{\int_{-x}^{x} e^{-\frac{(t)^2}{a}}.cos\,(2\pi ft)\,dt}{\int_{-\infty}^{+\infty} e^{-\frac{(t)^2}{a}}.cos\,(2\pi ft)\,dt} = \underbrace{\frac{2}{\sqrt{\pi}}\sum_{n=0}^{\infty}\frac{(-1)^n.A^{2n+1}}{n!2n+1}cos\big((2n+1)\theta\big)}_{\gamma(x,f)} \tag{23}$$

where:

$$\theta = arctan\left(\frac{\pi f a}{x}\right) \quad e \quad A = \sqrt{\frac{x^2}{a}+\pi^2 f^2 a} \tag{24}$$

This function is found repeatedly in the expansion of $\langle \psi_c, v\rangle_x$ and also relates to the truncating effect on the integral. The calculated amplitude $\hat{V}_{1H}$ under truncation conditions become

$$\hat{V}_{1H} \;= V_{1H.}\sqrt{1+\left(\frac{V_{2H}}{V_{1H}}\right)^2\beta^2(f)\,\gamma^2(x,f) - 2\beta(f)\,\gamma(x,f)\,\left(\frac{V_{2H}}{V_{1H}}\right)sin\theta} \tag{25}$$

Figure 6 shows how $\gamma(x,f)$ behaves as a function of the window half size *x*, for *f* = 1Hz, and having *a* as a parameter, for *a=0.5* to *1.2*, in steps of 0.1. In this plot, higher the value of a, higher the oscillations seen in $\gamma(x,f)$. As we see, $\gamma(x,f) \to 1$ for sufficiently large *x*, which is the ideal case, when if we truncate the integral or not does not matter for the filter calculation. However, severe errors may arise if the combination of *a* and *x* values does not lead to the desired $\gamma(x,f) \to 1$, since large values for $\gamma(x,f)$ will scale up the undesired β terms inside the square root, which combined with $V_{2H} \gg V_{1H}$ makes errors much larger.

An approximation for $\gamma(x,f)$ for larger *x* is derived in Shibuya (2009):

$$\gamma(x,f) \approx erf\left(\frac{x}{\sqrt{a}}\right) \tag{26}$$

where the function *erf* is the integral of a gaussian function with $\sqrt{a}$ as its standard deviation, so from $\frac{x}{\sqrt{a}} > 2.5$ to 3 we can be assure that $\gamma(x,f) \cong 1$. It then poses a superior limit for a to avoid windowing effects:

$$a_{max} \leq \left(\frac{x}{3}\right)^2 \tag{27}$$

Even though raising *a* is desirable because increases the filter selectivity and lowers $\beta(f)$, and reduces the influence of much larger V_{2H} on the V_{1H} measurement, this comes at expense of spreading the wavelet out of the windows boundaries, which leads to higher errors due to the truncation of the integral. This analysis show that to remedy this can only be accomplished by using higher values of the windows size *2x*, but that in turn reduces the rotation rate update and so the FOG bandwidth. The trade-off is that higher bandwidth means that we use smaller band-pass selectivity on the filter.

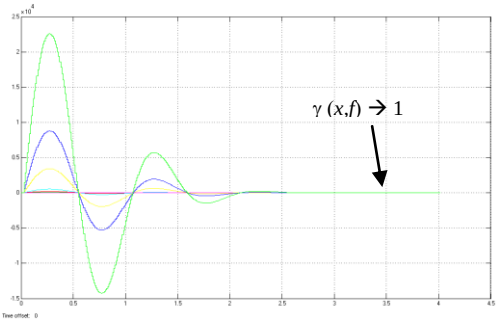

Figure 6. Plot of $\gamma(x,f)$, as a function of the window half size, x, for f = 1Hz, for several values of a, showing how the windowing effect works on the Morlet function band-pass filters. That effect ceases to be significant when $x > 3\sqrt{a}$.

We may say that the choice of the parameter a is the key factor on a compromise between accuracy and bandwidth/processing time. On the other hand, a larger value of *a* causes windowing effects which can be bettered by lowering the sensors bandwidth. Qualitatively speaking, we can see that if we choose a value for *a* smaller such that the Morlet function is well within the window frame, or else, it dies out at times close to the window center and far from the edges of the window, we avoid the windowing effect, but we have two other concerns in this case: first, lowering *a* may raise values for $\beta(f)$, and lower the filter selectivity, which in turn makes also more difficult to attain $\hat{V}_{1H} \cong V_{1H}$., since $V_{2H} \gg V_{1H}$. And second, due to the A/D converter precision, related to the A/D numbers of bits *N* used in the digitalization process, we may incur in another type of error: points not very far from the windows center do not contribute correctly in the sum because of cumulatively higher relative errors on their product with very small wavelet points, which may have died out below the A/D resolution level within the window.

So there is an optimal range for *a*. Taking into account this latest effect, it poses a lower limit for *a* values. When calculation is done considering the A/D number of bits *N*, its input voltage range $\Delta V_{ref} = V_{ref}^{+} - V_{ref}^{-}$, defined by its voltage rail references V_{ref}^{+} and V_{ref}^{-}, the desired signal-to-noise ratio *SNR*, in dBV, and the desired minimum value of V_{1H} we need to measure, we end up (Shibuya, 2009) with the range

$$\frac{1}{\pi^2 f_m{}^2}\left[\frac{SNR\,(dBV)}{20}.ln(10) + ln\left(\frac{\Delta V_{ref}}{2^{(N)}.V_{1Hmin}}\right)\right] < a < \left(\frac{x}{3}\right)^2 \tag{28}$$

Here f_m is the frequency of the modulation signal applied to the PM. Of course that relationship may not produce a valid interval to a for all desired values of V_{1Hmin} and SNR, for a given *N*. But will guide the choice of the Morlet filter to optimize the rotation rate measurement.

5. EFFECT OF HIGHER ORDER HARMONICS ON FILTER PERFORMANCE

So far we have represented the FOG photodetector signal $V(t)$ approximately as composed of mainly its first and second harmonics. Now we may proceed to investigate if that approximation is reasonable and quantify the effect of higher order harmonics on the V_{1H} measurement. Even though the harmonics amplitudes of higher order terms are much smaller than V_{2H}, because they are proportional to Bessel functions which are very small for a practical values of phase modulation index θ_m, their total contribution may or may not be negligible. For that, we may use the expansion up to the nth term, here assuming n to be even, without loss of generality:

$$V(t) = \sum_{k=0}^{\frac{n}{2}-1} V_{(2k+1)H}.sen\big((2k+1)\omega' t + (2k+1)\phi\big) + \sum_{j=1}^{\frac{n}{2}} V_{(2j)H}.cos\big((2j)\omega' t + (2j)\phi\big) \tag{29}$$

where, for FOG with phase modulation, we have

$$V_{(2k+1)H} = -J_{2k+1}(\theta_m).sen(\kappa\Omega), odd\ harmonics,\ \ k \geq 0 \quad (30)$$
$$V_{(2j)H} = J_{2j}(\theta_m).cos(\kappa\Omega), even\ harmonics,\ j \geq 1 \quad (31)$$

If we are to estimate what those extra harmonic content impacts on our previous results, we may find how much it is from the third harmonics on, as compared to the previous results. The dot product integrals working over those higher order harmonics produce the extra contributions CA_{ψ_s} and CA_{ψ_c} below:

$$CA_{\psi_s} = C_s.\sum_{k=1}^{\frac{n}{2}-1}\frac{V_{(2k+1)H}}{2}.\sqrt{\pi a}.cos\big((2k+1)\phi\big)\{\beta\big((2k+1)f' + f\big) - \beta\big((2k+1)f' - f\big)\} + C_s.\sum_{j=2}^{\frac{n}{2}}\frac{V_{(2j)H}}{2}.\sqrt{\pi a}.sen\big((2j)\phi\big)\{\beta\big((2j)f' + f\big) - \beta\big((2j)f' - f\big)\} \quad (32)$$

$$CA_{\psi_c} = C_c.\sum_{k=1}^{\frac{n}{2}-1}\frac{V_{(2k+1)H}}{2}.\sqrt{\pi a}.sen\big((2k+1)\phi\big)\{\beta\big((2k+1)f' + f\big) + \beta\big((2k+1)f' - f\big)\} + C_c.\sum_{j=2}^{\frac{n}{2}}\frac{V_{(2j)H}}{2}.\sqrt{\pi a}.cos\big((2j)\phi\big)\{\beta\big((2j)f' + f\big) + \beta\big((2j)f' - f\big)\} \quad (33)$$

Note that the higher arguments on the β functions are indeed very small, a further reason why they affect very little the V_{1H} measurement. By establishing the ratio between the impact on V_{1H} of higher harmonics to previous results we find the relative contributions ΔCA_{ψ_s} and ΔCA_{ψ_c}:

$$\Delta CA_{\psi_s} = \frac{\sum_{k=1}^{\frac{n}{2}-1} V_{(2k+1)H}.\{\beta((2k+2)f) - \beta((2k+2)f)\}}{V_{1H}.[\beta(2f) - \beta(0)]} \quad (34)$$

$$\Delta CA_{\psi_c} = \frac{\sum_{j=2}^{\frac{n}{2}} V_{(2j)H}.\{\beta((2j+1)f) + \beta((2j-1)f)\}}{V_{2H}.[\beta(3f) + \beta(f)]} \quad (35)$$

Figure 7 summarizes that relative contribution of higher harmonics, in percentage, from computational calculations over ΔCA_{ψ_s} and ΔCA_{ψ_c}. The plot is that percentage as a function of the phase modulation index θ_m. Also we include in the plot the Bessel functions $J_1(\theta_m)$ and $J_2(\theta_m)$, multiplied by a 20x factor, to plot all curves in a convenient fashion. We see that for usual values $\theta_m < 3$ radians (maximum sensitivity for $V_{1H} = KJ_1(\theta_m) * sin(k\Omega)$ occurs for $\theta_m =$ 1.84 radians, which is the maximum of the Bessel function $J_1(\theta_m)$, there is negligible contribution of less than 0.15% Exception already expected is around 3.7 radians, the first zero of $J_1(\theta_m)$, but at that region, as a consequence, there is no V_{1H} sensitivity and FOG´s cannot operate there, so it is not relevant.

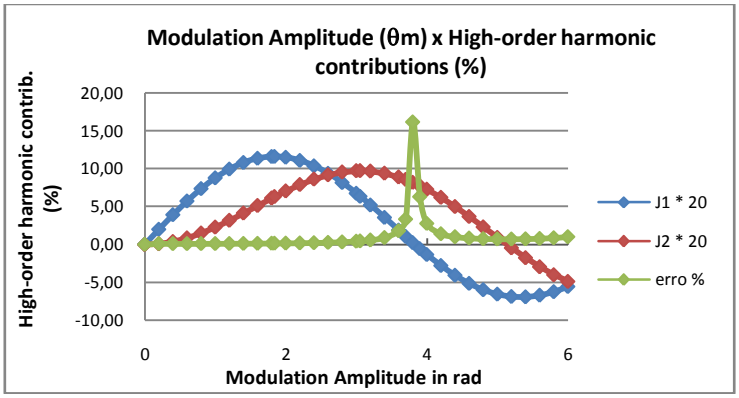

Figure 7. Plot of higher harmonics contribution as a function of the phase modulation index on the FOG´s PM.

6. IMPLEMENTATION AND RESULTS

The verification of the theory presented above take two steps: First, an independent and comprehensive simulation just calculating the dot product integrals under several different conditions was performed at MATLAB. Adjustable settings were the value of a, the ratio between V_{2H} and V_{1H} to check selectivity, A/D number of bits N, number M of

samples in the window, noise floor, and many others. The simulation was done to verify the expected performance under many conditions, and it used a frequency f of 1Hz. The results can be scaled to any other value of f and will remain the same if we set a as to keep the same value of $(a.f^2)$. Basically, three types of errors could be analyzed either independently or in combination:

- Harmonic Detection Crosstalk (HDC), the error induced by the fact that the pass-band filter still picks up some residuals from much larger V_{2H}.
- Signal to Noise Ratio (SNR), by setting noise levels with or without the presence of V_{2H}.
- Quantization error (QE), related to the sampling process and number of samples in the window.

We summarize some of the results here. Figure 8 below shows the influence (HDC) of V_{2H} on the V_{1H} measurement, using the A/D number of bits as a parameter, for 256 samples within the calculation window. There actually $V_{1H} = 0V$ and $V_{2H} = 1V$ are the inputs, and it shows the value that the filter would give, in this condition, as a function of a. As can be seen, optimum results would come up on a small interval around a=2, with a slight dependence on N. Area circled to the left presents errors related to the quantization process plus poor selectivity (large filter bandwidth picks up V_{2H}, so higher HDC), as discussed earlier on for lower values of a. Area circled to the right shows the error due to the windowing effect for larger values of a. Infinite number of bits means that no quantization was considered other than the basic one performed by the simulation software on its representation of samples.

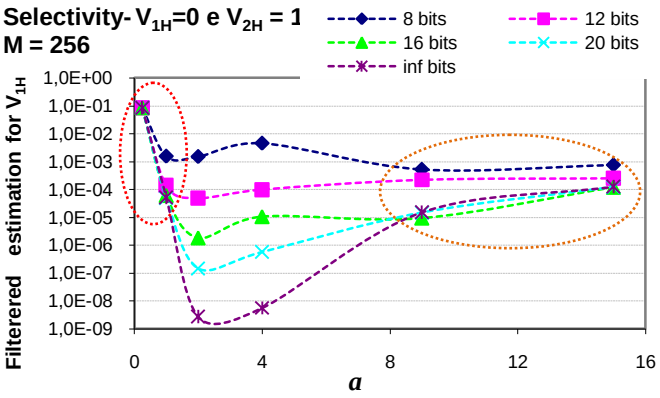

Figure 8 – Filter harmonic detection crosstalk, showing what the filter would give for when $V_{1H} = 0V$ and $V_{2H} = 1V$ are actually the inputs as a function of a, having the A/D number of bits N as a parameter.

Figure 9 shows a result for a input when V_{1H} was -80 dB below V_{2H}, with a 16 bits A/D, now using the number of samples M in the window as the parameter. The plot is the predicted percentage relative error in V_{1H} as a function of a. Again we see an optimum interval for a, for the same reasons discussed in the earlier plot. We calculate what would this interval be from the developed theory it gives $2.05 \leq a \leq 7.11$, which is in nice fitting to the observed in that plot.

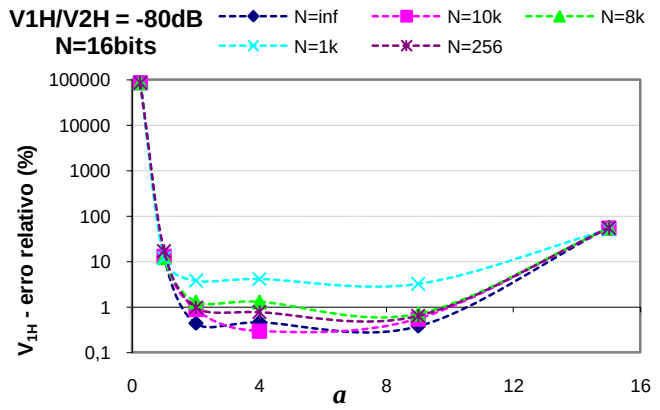

Figure 9 - Relative Error in V_{1H}

As the next step, a Morlet function filter implementation was done on an Analog Devices Tiger Shark TS201 platform, capable of doing 32 bit floating point calculations, which had a nominal 24 bit A/D converter operating at 48 kHz data sample frequency. The DSP hardware had a 10x gain pre-amplifier. Figure 10 shows the results when V_{1H} was

held constant at only $7\mu V$ and $V_{2H} = 0{,}7$V. The plot is of the measured $\hat{V}_{1H}$, in Volts, in successive computations. From there we see that there is room for measurements down to a few microvolts. Standard deviation is smaller than 0.5 μV.

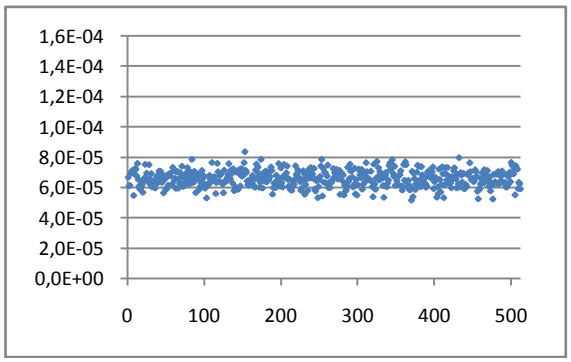

Figure 10 – DSP processor output for a 7μV input.

7. CONCLUSIONS

We implemented in a DSP platform a Morlet function digital signal processing to demodulate photodetector signals from fiber-optic gyros using optical phase modulation. The true band-pass filter developed was able to extract small amplitudes V_{1H} of the first harmonics, which is proportional to rotation rates in the lower Ω range, even in the presence of much larger second harmonics amplitude V_{2H} in ratios V_{2H}/V_{1H} larger than 90 dB. It shows better stability and range than custom analog circuitry based on lock-in amplifier techniques, with the integration advantages of digital implementations. The raw data was processed, with no significative pre-filtering, so a compact solution can be found to integrate all FOG axes demodulation electronics, and other functions as well, since the DSP may also be used for stability control of the laser source, parameter monitoring, data storage and signal generation for modulation, for example. This allows for more compact and rugged designs targeting space applications.

A theoretical development was also presented, which defined the calculations to be performed, pointed out its expected limitations, and estimated the optimum parameter choice for the Morlet function in FOG applications. Besides, it was demonstrated that disregarding higher order harmonics has negligible effect on the development of the filter theory presented. A simulated computation, which basically reproduces the DSP software, was run on MATLAB and showed good agreement with theoretical results.

8. REFERENCES

Carvalho, R. T., 1991 “Redução de Deriva em Giroscópios a Fibra Óptica convencional”, ITA, Tese de Mestrado em Engenharia Elétrica e Computação, São José dos Campos – Brasil

El-Sheimy, N.; Nassar, S.; Noureldin, 2004, A. “Wavelet de-noising for IMU alignment”, Aerospace and Electronic Systems Magazine, IEEE, Vol. 19, Issue 10, P. 32 – 39

Ezekiel, S., Arditty, H.J, 1982, “Fiber-optic Rotation Sensors and Related Technologies”, Springer Series in Optical Sciences, vol. 32, Springer-Verlag, New York

Farrel, J. A, Barth, M., 1998, “The Global positioning System & Inertial Navigation”, MacGraw-Hill

Lefèvre, H., 1993, The Fiber-Optic Gyroscope, Artech House Inc., Boston, MA.

Post, E. J.,1967, "Sagnac effect", Rev. Mod. Phys., Vol. 39, P. 475-494

Sagnac, G., 1923 "L'éther lumineux démontré par l'effet du vent relatif d'éther dans un interféromètre en rotation uniforme", C. R. Acad. Sci., Vol. 95, P. 708-710

Shibuya, L.H., 2008, “Sintese de Filtros digitais para demodulação de sensores inerciais com modulação de fase óptica”, ITA, Tese de Mestrado em Engenharia Eletrônica e Computação, São José dos Campos, Brasil.

Vali ,V., Shorthill R., 1976, "Fiber ring interferometer", App. Opt., Vol. 15, P. 1099.

9. RESPONSIBILITY NOTICE

The authors are the only responsible for the material included in this paper.